Journal of Colloid and Interface Science xxx (xxxx) 141054

Contents lists available at ScienceDirect

Journal of Colloid and Interface Science

journal homepage: www.elsevier.com

Structure and stability of styrene-maleic acid lipid particles: the role of polymer-lipid ratio

Bridget Tang [a], Philip Kitchen [a], Luke M. Broadbent [a], Steven D. Quinn [b, c], Nawal Hassan [a], Siriporn Chaimueangchuen [a], Barbara Gerbelli [d], Katsuaki Inoue [d], Nathan Cowieson [d], Fátima Herranz-Trillo [e], Alice J. Rothnie [a, f], Roslyn M. Bill [a, f, g], Paul D. Topham [a, h], Alan D. Goddard [a, f], Jacob J.K. Kirkensgaard [i, j, **], Matthew J. Derry [a, h, *], Andreas Haahr Larsen [i, ***]

[a] Aston Institute for Membrane Excellence, Aston University, Birmingham, B4 7ET, UK
[b] School of Physics, Engineering and Technology, University of York, York YO10 5DD, UK
[c] York Biomedical Research Institute, University of York, York YO10 5DD, UK
[d] Diamond Light Source, Harwell Science and Innovation Campus, Didcot OX11 0DE, UK
[e] MAX IV Laboratory, Lund University, Fotongatan 2, 22484 Lund, Sweden
[f] Department of Biosciences, School of Medicine, Pharmacy and Biosciences, Aston University, Birmingham, B4 7ET, UK
[g] Department of Physiology, Anatomy and Genetics, University of Oxford, Oxford OX1 3PT, UK
[h] Department of Chemical and Bioprocess Engineering, School of Engineering and Innovation, Aston University, Birmingham, B4 7ET, UK
[i] Niels Bohr Institute, University of Copenhagen, DK-2100 Copenhagen Ø, Denmark
[j] Department of Food Science, University of Copenhagen, DK-1958 Frederiksberg C, Denmark

ARTICLE INFO

Keywords:
Membrane solubilization
Amphiphilic copolymers
Polymer-lipid particles
Nanodiscs
Small-angle X-ray scattering
Biophysics
SMALPs

ABSTRACT

Amphiphilic copolymers have emerged as powerful, detergent-free tools for solubilizing biological membranes, enabling the extraction and stabilization of membrane proteins within native-like lipid environments. We report a comprehensive, multi-technique elucidation of how polymer:lipid stoichiometry governs the formation, size, and stability of styrene-maleic acid lipid particles (SMALPs). Using commercial SMA2000, a styrene-maleic acid copolymer made using free radical polymerization and 1,2-ditetradecanoyl-*sn*-glycero-3-phosphocholine (DMPC) as a model phospholipid, we prepared SMALPs across a wide range of polymer-to-lipid weight ratios and employed an integrated suite of orthogonal characterization methods, including size exclusion chromatography (SEC), dynamic light scattering (DLS), flow-induced dispersion analysis (FIDA), mass photometry, ensemble and time-resolved Förster resonance energy transfer (FRET), and small-angle X-ray scattering (SAXS), to establish the structural consequences of varying polymer content. Our data reveal that efficient lipid solubilization into nanodiscs requires a minimum amount of polymer. Above ~1% (*w/v*) SMA2000: 1% DMPC, well-defined nanodiscs of ~10 nm diameter are formed that, on average, exhibit a consistent stoichiometry of ~130 lipids encircled by ~11 polymer chains. Through a new molecularly-constrained SAXS model, we show that these nanodiscs possess a stable bilayer height across variations in polymer to lipid ratio and a narrow polymer belt, and that their structural parameters remain invariant once excess polymer is used. In contrast, insufficient polymer (< 1% *w/v*) generates bimodal populations including substantially larger discs. Notably, nanodiscs formed at optimal polymer:lipid ratios remain structurally stable for at least two months. Together, these results provide a rigorous quantification of SMALP composition and preferred size, enhancing our understanding of polymer-lipid nanodisc formation and offering critical design rules for detergent-free membrane protein extraction.

* Corresponding author at: Aston Institute for Membrane Excellence, Aston University, Birmingham, B4 7ET, UK.
** Corresponding author at: Niels Bohr Institute, University of Copenhagen, DK-2100 Copenhagen Ø, Denmark.
*** Corresponding author.
E-mail addresses: jjkk@nbi.ku.dk (J.J.K. Kirkensgaard), m.derry@aston.ac.uk (M.J. Derry), larsen@nbi.ku.dk (A.H. Larsen).

https://doi.org/10.1016/j.jcis.2026.141054
Received 30 March 2026; Received in revised form 29 June 2026; Accepted 1 July 2026
0021-9797/

1. Introduction

Membrane proteins play crucial roles in cellular function, acting as transporters, receptors and structural components [1]. To better understand their structure and function, it is often necessary to purify them from the hydrophobic lipid membrane. Membrane protein purification methods typically utilize detergents to solubilize the protein, stripping away its native lipid environment [2,3]. In 2009, an alternative approach for solubilization of membrane proteins was reported using a styrene-maleic acid copolymer (SMA) [4]. SMA is an amphiphilic copolymer comprising hydrophobic styrene (S) moieties and hydrophilic maleic acid (MA) groups, with varying styrene-to-maleic acid molar ratios enabling fine tuning of the hydrophobic/hydrophilic balance [5]. Although direct copolymerization of S and MA has been recently reported [6,7], SMA is typically synthesized via the copolymerization of styrene and maleic anhydride (MAnh), followed by hydrolysis of the subsequent styrene-maleic anhydride copolymer (SMAnh) to yield SMA [7–11]. Due to electronic effects arising from the electron-rich phenyl ring of styrene and the electron-poor double bond of maleic anhydride, alternating copolymerization of S and MAnh is favoured [12,13].

The most widely used polymer and most effective for extraction of many membrane proteins is commercial SMA2000 [4] which is synthesized via the free radical polymerization of S and MAnh and subsequent hydrolysis to yield SMA with a 2:1 S:MA molar ratio, where the S and MA units are distributed throughout the chains statistically. Due to the nature of its synthesis, SMA2000 has a broad molecular weight distribution that contains polymer chains that vary substantially in length and monomer sequence [6,8]. Amphiphilic polymers can solubilize lipid bilayers, generating nanodiscs in which lipids are encircled by a polymer belt. This enables the direct extraction of membrane proteins from cell membranes while preserving patches of native lipids around them [4]. SMA has proven to be effective for the extraction of membrane proteins while retaining their structure and activity [14–17]. SMA-based lipid nanoparticles are commonly termed SMALPs (styrene-maleic acid lipid particles) [18], although they are also referred to as lipodisqs™ [19], native nanodiscs, [20] polymer lipid particles (PLPs) [21] or polymer lipid discs (PLDs) [22].

In addition to SMAs, other commercially available amphiphilic polymers can be used for this purpose such as copolymers of acrylic acid-styrene (AASTY) [23], diisobutylene-maleic acid (DIBMA) [14,24] and polymethacrylates (PMAs) [25]. Recently, synthesis of rationally designed polymers for extraction of membrane proteins has accelerated. Most notably, controlled polymerization techniques such as reversible addition-fragmentation chain transfer (RAFT) polymerization have been used to synthesize suitable copolymers with multiple blocks, controlled molecular weights and corresponding lower dispersity compared to traditional free radical polymerization [7–9,26,27].

This study focuses on the most commonly used polymer for membrane protein solubilization, SMA2000, and a simple synthetic lipid, 1,2-ditetradecanoyl-*sn*-glycero-3-phosphocholine (DMPC), to generate model polymer-lipid nanoparticles. DMPC has been widely used as a model lipid with which to test polymer-mediated solubilization, which allows for comparison of our findings with published data [19]. SMALPs have been investigated extensively [7,18,28–31] and it has been reported that changing the polymer-to-lipid ratio during the disc formation may facilitate the accommodation of larger proteins within a SMALP [9]. However, there is limited evidence that SMALPs formed using less than 2% *w/v* polymer are stable, and it is unknown how higher polymer concentrations (above 3% *w/v*) affect structure, size and stability. Furthermore, although the number of lipids in SMALPs formed from SMA2000 and DMPC has been reported to be around 140 [18], the precise lipid:polymer stoichiometry favoured when forming stable SMALPs is unknown. We present a rigorous study employing a suite of characterization techniques including optical dentisty, size exclusion chromatography (SEC), dynamic light scattering (DLS), flow-induced dispersion analysis (FIDA), mass photometry, Förster resonance energy transfer (FRET) and size exclusion chromatography coupled with small-angle X-ray scattering (SEC-SAXS) to address these questions (Fig. 1).

2. Experimental

2.1. Materials

SMA2000 polymer was provided by Cray Valley and was supplied as styrene-maleic anhydride copolymer. SMA2000 was hydrolysed and characterised following the procedure outlined in the Supporting Information, Section S1. Dimethyl sulfoxide (DMSO), hydrochloric acid (HCl), trizma base and NativeMark™ unstained protein standard were purchased from Fisher Scientific. Sodium hydroxide (NaOH) was pur-

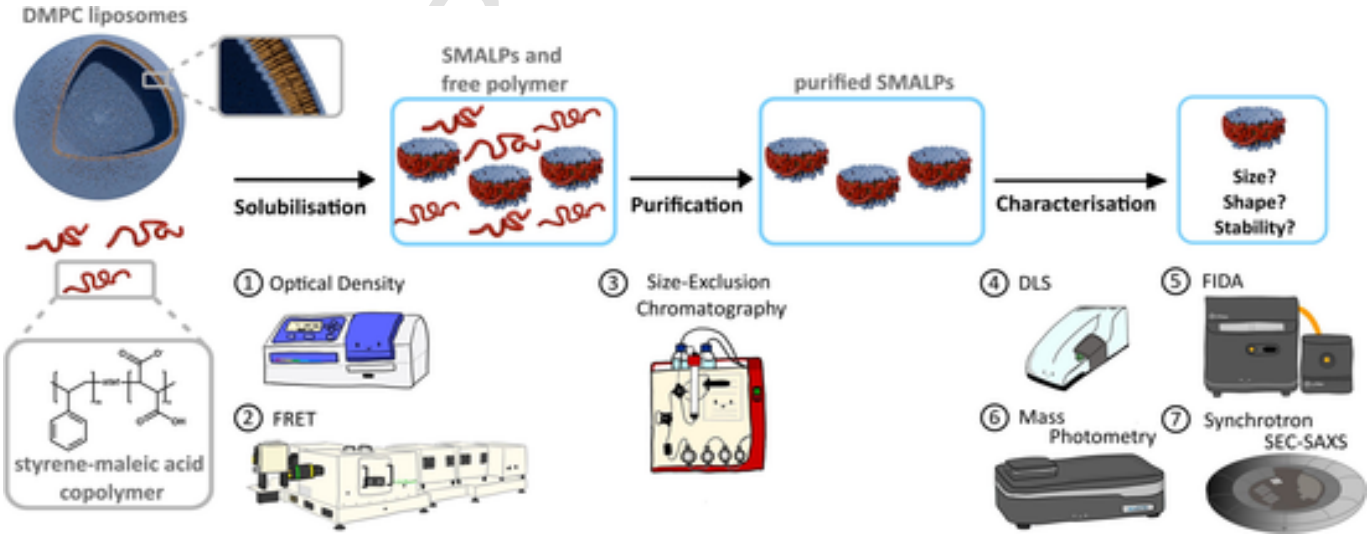

Fig. 1. Overview of synthesis and characterization of polymer-lipid nanoparticles. DMPC was solubilized with varying concentrations of SMA2000 which was monitored using optical density (1) and FRET (2). Polymer-lipid nanoparticles were purified using SEC (3). Characterization of size, shape and stability was achieved using DLS (4) FIDA (5) mass photometry (6) and synchrotron SEC-SAXS (7).

chased from Sigma. 1,2-Dimyritoyl-*sn*-glycero-3-phosphocholine (DMPC) was purchased from Avanti Polar Lipids Inc. Sodium chloride >99.0% (NaCl) was purchased from Duchefa Biochemie B.V. Lipophilic membrane stains (1′-dioctadecyl-3,3,3′,3′-tetramethylindocarbocyanine perchlorate (DiI) and 1,1′-dioctadecyl-3,3,3′,3′-tetramethylindodicarbocyanine, 4-chlorobenzenesulfonate salt) (DiD)) were purchased from Thermo Fisher Scientific. All stock solutions were stored at −20 °C prior to use. Deuterium oxide (D_2O) and trimethylsilyl propanoic acid (TSP) was purchased from Cambridge Isotope Laboratories Inc. MemGlow 488 was purchased from Cytoskeleton Inc. Phosphate-buffered saline (PBS) tablets were purchased from Gibco. All chemicals were used as supplied unless specified.

2.2. Preparation of buffer, liposomes, polymer solutions and lipid solubilization

Buffer was prepared by dissolving 20 mM trizma base and 150 mM NaCl in ultra-pure water. The pH was adjusted to 8 using HCl. The buffer was then filtered using 0.22 μm polyethersulfone (PES) membrane. 20 mg/mL DMPC was suspended in buffer and left to shake at 37 °C (above the phase transition temperature of 24 °C) for 1 h to form multilamellar liposomes. Hydrolysed SMA2000 was dissolved in buffer to make polymer solutions at different concentrations: 10, 6, 5,4, 3, 2 and 1, where all concentrations stated are % *w/v*. 500 μL SMA2000 polymer solution was mixed with 500 μL DMPC liposomes forming final concentrations of 5:1, 3:1, 2:1, 2:1, 1.5:1, 1:1 and 0.5:1 of SMA2000: DMPC, respectively. All concentrations stated are in % w/v.

2.3. Optical density

The liposome solubilization induced by SMA2000 was monitored by measuring the optical density of 400 nm light using a Jenway 6300 single-beam spectrophotometer. Buffer was used as a calibrant. 500 μL liposome (20 mg/mL) was added to semi-micro cuvettes and allowed to equilibrate for 30 s before the addition of SMA2000 solution, as stated above. All measurements were followed over 2 min. All measurements were performed at 21 °C.

2.4. Preparation of liposomes for Förster resonance energy transfer (FRET): incorporating the DiI and DiD sensors

200 nm sized DMPC liposomes containing 0.1 mol% DiI, 0.1 mol% DiD and 99.8 mol% DMPC were prepared by extrusion, as previously described [32–34]. Briefly, lipids, DiI and DiD were mixed in chloroform before the solvent was evaporated under gentle nitrogen flow. The dried lipid film was then resuspended in 50 mM Trizma-base buffer (pH 8) and vortexed. Large (200 nm) unilamellar liposomes were then prepared using a Mini Extruder (Avanti Polar Lipids) where the solutions were extruded 21 times through a polycarbonate membrane filter with 200 nm size cut off. As previously reported, the incorporation of 0.1 mol% DiI and 0.1 mol% DiD into the liposomes produces a FRET efficiency per liposome (E) of ~0.5[32–34] as each liposome contain dyes spatially separated by ~5.2 nm apart, therefore variations in E enables the quantification of structural rearrangements such as swelling or compaction, in either direction.

2.5. Steady state fluorescence and FRET spectroscopy

Fluorescence emission spectra were measured under 532 nm excitation and magic angle conditions with a FluoTime 300 spectrophotometer equipped with a PMA Hybrid 07 photomultiplier tube (Picoquant). All spectra were acquired using an integration time of 0.1 nm per second and all measurements were performed with a final DMPC concentration of 25 μg/mL in buffer. Apparent FRET efficiencies (E) were estimated as $E = I_A/(I_A + I_D)$ where I_D and I_A represent the fluorescence emission intensities of DiI and DiD at 565 and 665 nm, respectively. DiI-DiD separation distances (R) were then estimated via

$$R = \sqrt[6]{R_0^6\left(\frac{1}{E} - 1\right)} \quad (1)$$

where R_0 is the Förster radius (5.2 nm) [32].

2.6. Time correlated single photon counting

Time-resolved fluorescence spectroscopy on fluorescently labelled liposomes was performed using the same FluoTime300 spectrophotometer as outlined previously. Time-resolved fluorescence decays were measured under magic angle conditions using pulsed excitation at 532 nm (LDH-D-FA-530 L, Picoquant) with a repetition rate of 64 MHz. Fluorescence emission decays at 565 nm, corresponding to the peak of DiI emission, were collected until 10^4 counts accumulated at the decay maximum. Fluorescence decay curves were fitted by iterative reconvolution of the instrument response function and the observed fluorescence decay using a bi-exponential decay function of the form $I_t(t) = Ae^{-\frac{t}{\tau_1}} + Be^{-\frac{t}{\tau_2}}$ where, t is time, τ_1 and τ_2 represent the fluorescence lifetime components of the decay and A and B are the associated amplitudes. Amplitude-weighted average lifetimes were then calculated as $\tau = \frac{A\tau_1^2 + B\tau_2^2}{A\tau_1 + B\tau_2}$. The quality of the fit was judged by the reduced χ^2. All experiments were performed in 50 mM Trizma-base buffer (pH 8) with a final DMPC concentration of 25 μg/mL. The polymer-to-lipid ratio was varied from 0.5–5.0 SMA2000: 1 DMPC by adding 25–250 μg/mL of SMA2000. Instrumental response functions were acquired from water solutions containing Ludox beads.

2.7. Size exclusion chromatography (SEC)

SEC was used to separate the polymer-lipid nanoparticles from the free polymer. 500 μL sample was loaded onto a Superdex 200 10/300 column equilibrated in buffer. A wavelength of 260 nm was chosen to detect species passing through the SEC column because styrene absorbs UV light around 260–280 nm. The column was run at flow rate of 0.5 mL/min and 0.2 mL fractions were collected for further analysis. Fractions from the first peak at elution volume 12 mL (peak 1) corresponding to polymer-lipid nanoparticles were pooled. Fractions from a smaller polymer-lipid nanoparticles population at 14 mL (peak 2) were also collected. All measurements were performed at 4 °C.

2.8. Dynamic light scattering (DLS)

DLS measurements were conducted using a Zetasizer NanoZS instrument (Malvern Panalytical, UK) equipped with a 4 mW He—Ne laser operating at a wavelength of 633 nm and a fixed scattering angle of 173°. Purified polymer-lipid nanoparticles corresponding to peak 1 at a 12 mL elusion volume from the SEC were run neat after collection. Polymer-only was dissolved at the solubilization concentration in buffer and filtered before DLS analysis. Buffer was used as the solvent with a refractive index of 1.332. All measurements were performed at 21 °C. The polydispersity index and z-average diameter were calculated by cumulant analysis of the correlation function using Dispersion Technology Software version 6.20 and data were averaged over three sets of approximately thirteen runs each of 30 s duration. All correlograms can be found in the Supporting Information (see Section S5).

2.9. Flow-induced dispersion analysis (FIDA)

Purified polymer-lipid nanoparticles corresponding to SEC peak 1 were analysed by FIDA using a Fida1 instrument (Fidabio). SMALPs were labelled using MemGlow 488 membrane stain by firstly diluting a 20 μM DMSO solution of MemGlow 488,100-fold into Tris buffer at

pH 8, followed by immediate tenfold dilution into the SMALP sample, to give final concentrations of 20 nM MemGlow 488 and 0.1% *v*/v DMSO. The FIDA measurements were made using a 100 mm × 75 μm uncoated capillary and a 480 nm detector module. The capillary was pre-rinsed with filtered buffer (20 mM Tris base, 150 Mm NaCl) at pH 8, followed by injection of the labelled SMALP at 50 mbar for 10 s, and mobilisation using buffer at 400 mbar for 3 min. All measurements were performed at 21 ˚C. Hydrodynamic radii were fitted to the resulting fluorescence intensity timeseries using FIDA Analysis software (Fidabio) [36].

2.10. Mass photometry

Purified polymer-lipid nanoparticles corresponding to SEC peak 1 were analysed using a Refeyn MPTwo mass photometer. Samples were pre-diluted to approximately 100 nM in PBS, then diluted tenfold into a PBS droplet on the photometer stage to give a final concentration of approximately 10 nM. Data were collected for 60 s, with the image size set to "regular". All measurements were performed at 21 ˚C. The NativeMark™ unstained molecular weight marker (Thermo Fisher Scientific) was used for mass calibration. Gaussian distributions were fitted to the mass histograms using Refeyn DiscoverMP software, and data are reported as the mean and standard deviation of the fitted distribution.

2.11. Small-angle X-ray scattering (SAXS) data collection and reduction

SAXS data were measured at the B21 beamline at Diamond light source [35] (proposal sm39511–1) with wavelength (λ) of 0.095 nm, and sample to detector distance of 3.69 m giving a q range of 0.045 to 3.4 nm^{-1} with q defined as $4\pi\sin(\theta)/\lambda$, where 2θ is the scattering angle. The intensity was absolute calibrated against water. Samples were measured at 21 ˚C in 1.5 mm capillaries. SMA2000 samples without lipids were measured in batch mode using an EMBL Bio-SAXS (Arinax) sample handling robot. Batch-SAXS and SEC-SAXS data were reduced using the DAWN program [36]. The average and subtract process for the batch data were performed by B21 Python scripts. The errors were assessed using BayesApp [37]. SMALPs were measured in SEC-SAXS mode. Purified SMALPs from SEC peak 1 and SEC peak 2 were concentrated from 3 mL to around 100–200 μL using a Amicon® Ultra Centrifugal filter with 10 kDa cutoff and injected into an Agilent HPLC system with a Superdex 200 Increase 5/150 GL column mounted. The column was preequilibrated in buffer and run at a flowrate of 0.75 mL/min while measuring, Based on the findings, the errors were reprocessed using maximum likelihood [38]. SEC-SAXS data were reduced using bioXtas RAW [39], with linear baseline correction [40]. Frames were taken from the right side of the scattergram peak, where the calculated radii of gyration generally displayed a stable plateau. The first points in data (approximately 50) were affected by the beamstop and removed. The remaining data were rebinned logarithmically, to ensure proper sampling of each q-value, from around 2500 points to around 150 points. Reduced available at github.com/andreashlarsen/Tang2026. Any other data can be provided upon request. Pair distance distributions, $p(r)$, were generated by Bayesian indirect Fourier transformation as implemented in BayesApp [41], with default parameters. SAXS data were fitted in BayesFit [42,43] and all data fitting information can be found in the Supporting Information (Section S6).

3. Results and discussion

3.1. Structure and solution behaviour of hydrolysed SMA2000

The SMAnh polymer was hydrolysed to form the acid groups and the process was validated by FTIR and ^{1}H NMR (see Supporting Information, Section 2). The hydrolysed SMA2000 was prepared in various concentrations from 0.5% (5 mg/ml) to 5% (50 mg/ml) in buffer at pH 8 for solution behaviour characterization with DLS (see Supporting Information, Section S5.1) and SAXS (see Supporting Information Section S6.2). We found that the polymers formed assemblies of 2–3 polymer chains in line with previous studies [31], with an average diameter of around 3 nm, which was verified by DLS . At high concentration we observed static repulsion but no aggregation, whereas at low concentrations no repulsion was observed but the polymers formed larger aggregates. Repulsion has previously been observed for SMA2000 in solution and depends on concentration and ionic strength of the buffer [44]. Aggregation has also been observed in SAXS of SMA31, and at low concentrations, the aggregates are more prominent. This observation suggests that optimal SMALPs self-assembly conditions involve high SMA2000 concentrations, as non-aggregated polymers more readily interact with lipid bilayers, consistent with reports that SMALPs are formed with an excess of SMA2000 [45]. See Supporting Information for detailed breakdown and structural analysis and solution behaviour of hydrolysed SMA2000 alone.

3.2. Formation of polymer-lipid nanoparticles

Excess polymer has been widely shown to interfere with downstream processes such as affinity column binding and sodium dodecyl sulphate polyacrylamide gel electrophoresis (SDS-PAGE) [46] but there is also likely a minimum amount of polymer required for efficient solubilization. Therefore, DMPC liposomes were solubilized using varying SMA2000 concentrations of 0.5% *w/v* to 5% w/v with a fixed DMPC concentration of 1% w/v. Optical density measurements were used to investigate the dynamics of the SMA2000-lipid nanoparticle formation, by monitoring the changing turbidity during self-assembly. The kinetics traces (Fig. 2(a)) suggest the amount of polymer added influences how quickly the liposomes are solubilized. Therefore, the optical density data were plotted as ln(Absorbance) vs. time and fitted with a log-linear function to obtain the apparent initial solubilization rate constant (k_{app}) (all raw data and k_{app} curves are shown in the Supporting Information, see Section S3). The apparent rate of solubilization of DMPC increases monotonically with the increase in concentration of SMA2000 (Fig. 2 (b)). However, optical density measurements alone provide limited insight into morphological changes in the liposome, beyond indicating the reduction in particle size once SMA2000 is added.

To gain molecular-level insights into the SMA-liposome disruption process, ensemble steady-state and time-resolved FRET measurements were performed. For precursor liposomes, the DiI and DiD chromophores are in close proximity to one another (~5 nm), which, upon donor excitation, results in the fluorescence emission of DiI being quenched. By contrast, sensitized DiD fluorescence is high upon donor excitation because of non-radiative energy transfer. As the SMA2000:DMPC molar ratio was increased from 0 to 2, a progressive increase in DiI emission was observed alongside a corresponding decrease in sensitized DiD emission (Fig. 3(a)) [32–34]. A plateau of DiI emission was observed when the SMA2000:DMPC molar ratio was increased from 2 to 5, suggesting that the changes in morphology had stabilised. Overall, the donor and acceptor emission intensities were anti-correlated across the titration (Fig. 3(a)), which is a classic hallmark of FRET. To further confirm an energy transfer mechanism, the fluorescence lifetime of DiI in the presence of DiD extracted from time-resolved fluorescence decays (Fig. 3(b) and Fig. 3(c)) was evaluated under matched experimental conditions. The amplitude-weighted average lifetime of DiI progressively increased as a function of increasing SMA2000, consistent with a progressive de-quenching of DiI and a corresponding decrease in E (Fig. 3(d)). This is also indicative of morphological changes as the dyes become further apart suggesting that SMA2000 disrupts the liposome and isolates lipid patches from one another. The decays were best fitted to a bi-exponential model after reconvolution with the instrumental response function which likely represents different molecular environments associated with DiI. In the ab-

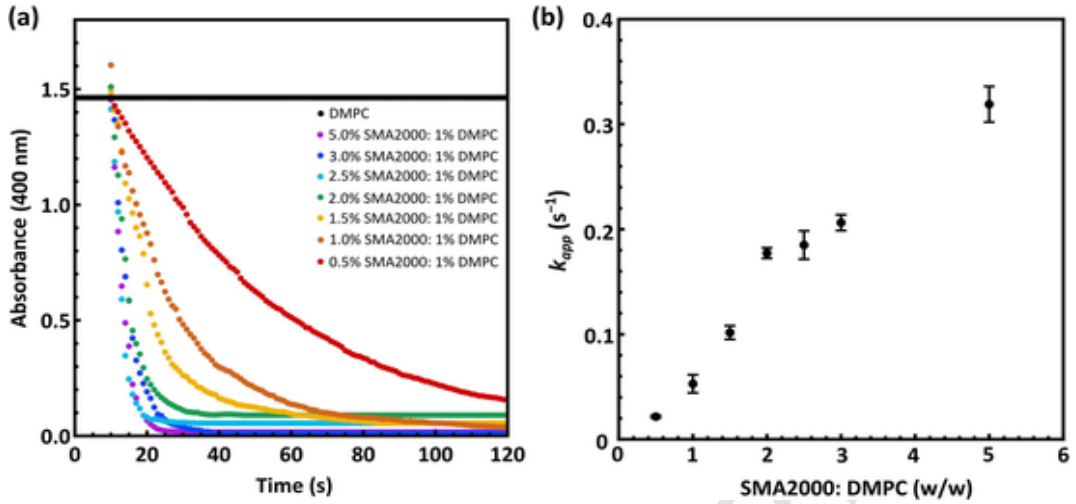

Fig. 2. (a) Solubilization of DMPC liposomes with varying concentrations of SMA2000 monitored by optical density measured at 400 nm and (b) effect of SMA2000 concentration on the apparent solubilization rate constant, k_{app}. Data points represent the mean value from 3 replicates and error bars represent the standard deviation.

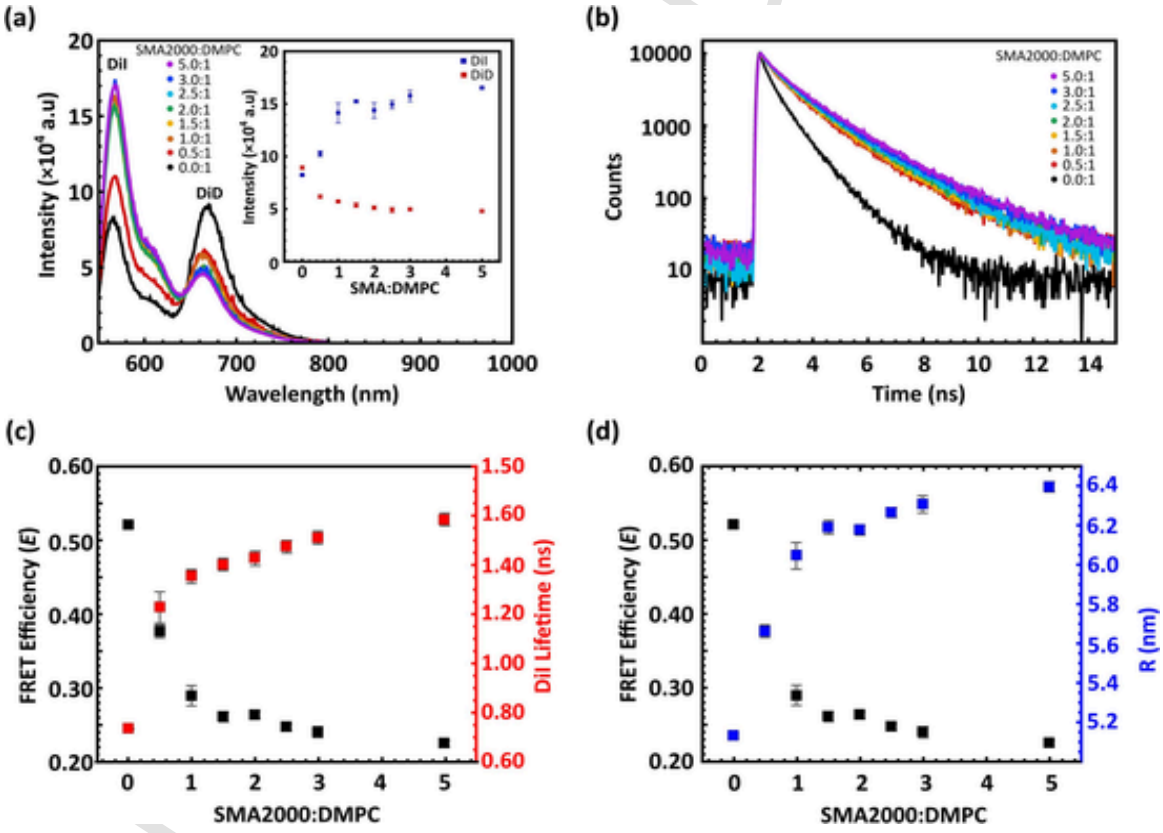

Fig. 3. (a) Representative variation in the fluorescence emission spectra of DMPC liposomes containing DiI (0.1%) and DiD (0.1%) as a function of the SMA2000:DMPC ratio. Inset: variation in the mean DiI and DiD emission intensities. (b) Corresponding representative variation in the time-resolved fluorescence decays obtained from DiI (l_{ex} = 532 nm, l_{em} = 565 nm). (c) Variation in the apparent FRET efficiency (black) and amplitude-weighted average lifetime of DiI (red) across the titration. Also shown in (d) is the variation in DiI-DiD separation distance (blue). Data points represent the mean and error bars represent the standard error of the mean from three replicates. (For interpretation of the references to colour in this figure legend, the reader is referred to the web version of this article.)

sence of any SMA2000, the liposomes displayed a mean FRET efficiency of ~0.52 and DiI displayed an average lifetime of 0.73 ns, consistent with a quenched state due to non-radiative energy transfer to DiD. As the SMA2000:DMPC molar ratio then increased in favour of SMA2000, the recorded FRET efficiency progressively decreased to values of ~0.38 and ~ 0.22 at SMA2000:DMPC ratios of 0.5 and 5, respectively. Similarly, the DiI lifetimes progressively increased to 1.23 ± 0.06 ns and 1.58 ± 0.03 ns under the same respective conditions (Fig. 3(d)). These data also indicate a progressive increase in the mean DiI-DiD separation distance which increased by ~25% to a final value of 6.4 nm. Taken together these data are supportive of substantial morphological changes within single liposomes during the SMA2000 interaction. However, FRET alone is insufficient to determine conclusively the morphology of the final product resulting from the interactions of SMA2000 with liposomes and further analysis was therefore required.

3.3. Isolation and analysis of polymer-lipid nanoparticles and free polymer

After solubilization, the solution contained a mixture of species including polymer-lipid nanoparticles and free polymer. Therefore, size exclusion chromatography (SEC) was used to fractionate the dominant polymer-lipid nanoparticle population (peak 1) from free polymer (see Supporting Information, Section S4). Fig. 4 shows the SEC chromatograms of polymer lipid nanoparticles formed using different concentrations of SMA2000. The peak eluting at ~12 mL (peak 1, highlighted in pink) shifted slightly to the left for samples prepared using less than 1% *w/v* SMA2000, suggested that these nanodiscs were larger. For samples made using ≤1% w/v SMA2000, the intensity of the peak decreased, indicating that there could be fewer polymer-lipid nanoparticles formed when not enough polymer is used. The peak at ~17.5 mL (peak 3, highlighted in blue) corresponds to the free polymer as expected. The intensity of the free polymer peak decreases as the polymer concentration decreases. However, even at the lowest concentration 0.5% w/v SMA2000 there was still free polymer present. At higher concentrations, another peak emerged at an elution volume of ~14.5 mL (peak 2, highlighted in green) from distinct polymer-lipid nanoparticles, different from the dominant population in peak 1. We will discuss this further below.

3.4. Characterization of polymer-lipid nanoparticle: diameter

To probe overall size, DLS and FIDA were used. Lipid nanoparticles were isolated and collected based on the fractions from SEC peak 1 (Fig. 4, highlighted in pink) and combined for further characterization. DLS was performed without any further purification or dilution (approximately 0.5% *w/v* solids). The DLS data (Fig. 5 and Table S5.2) show that the polymer-lipid nanoparticles prepared using >1% SMA2000 had a hydrodynamic diameter ~ 10 nm (PDI ~ 0.1) but when 0.5% SMA2000 was used the particles produced had a hydrodynamic diameter of ~20 nm (PDI = 0.18). This was compared with the average hydrodynamic diameter of DMPC liposomes using extruded 200 nm filters (~200 nm, PDI = 0.10) (Fig. 5(a)). Overall, the polymer-lipid nanoparticles had a hydrodynamic diameter at least twice that of the average hydrodynamic diameter of polymer aggregates alone, which was ~4 nm (PDI = 0.25) (Fig. 5(c)). The Flow-induced dispersion analysis (FIDA) [47] data also showed that polymer-lipid nanoparticles produced using >1% SMA2000 had a hydrodynamic diameter between 8 and 11 nm. Using less polymer, such as 0.5% SMA2000, polymer-lipid nanoparticles had a diameter of ~21 nm. Overall, the hydrodynamic diameters of the polymer-lipid nanoparticles measured using DLS and FIDA were in agreement as shown in Fig. 5(c-d). Both DLS and FIDA data suggest larger particles were formed when less polymer was used which also aligns with our SEC data and with previous observations in the literature [9,28,30].. Even though DLS and FIDA are both robust techniques for particle size measurements, their main limitation

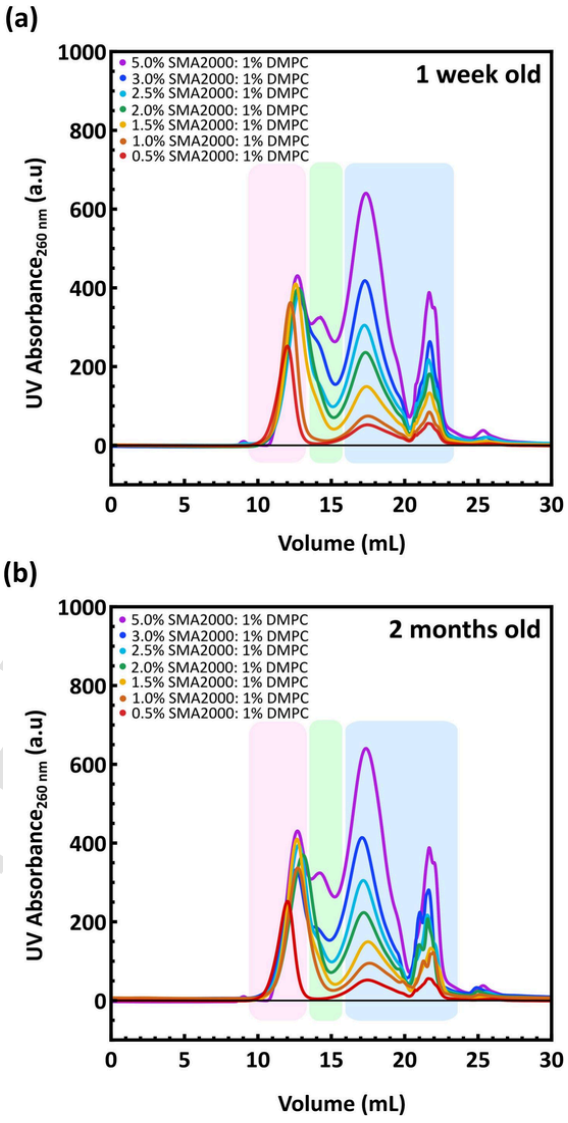

Fig. 4. (a) Size-exclusion chromatography of polymer lipid nanoparticles (1 week old) and (b) size-exclusion chromatography of polymer lipid nanoparticles (2 months old) measured at wavelength = 260 nm. Peak 1 highlighted in pink corresponds to the polymer-nanoparticles, Peak 2 highlighted in green corresponds to an unknown species and Peak 3 highlighted in blue corresponds to the free polymer. (For interpretation of the references to colour in this figure legend, the reader is referred to the web version of this article.)

is that both use the Stokes-Einstein equation to estimate the hydrodynamic diameter. The hydrodynamic diameter is by definition the diameter of an ideal hard sphere that diffuses in solution. Therefore, this model may not be the most appropriate method in determining the size of a non-spherical polymer-lipid particle.

3.5. Characterization of polymer-lipid nanoparticles: mass and multimodal distributions

Having established average particle diameters, mass photometry, a single-particle light scattering technique, was employed to investigate whether the size distribution represented multiple species. Fig. 6 shows a stacked plot of mass photometry data for polymer-lipid nanoparticles produced at various SMA2000 concentrations. Between 1% and 3% polymer, a single population of particles was present with masses between 103 kDa and 132 kDa. However, when a high concentration

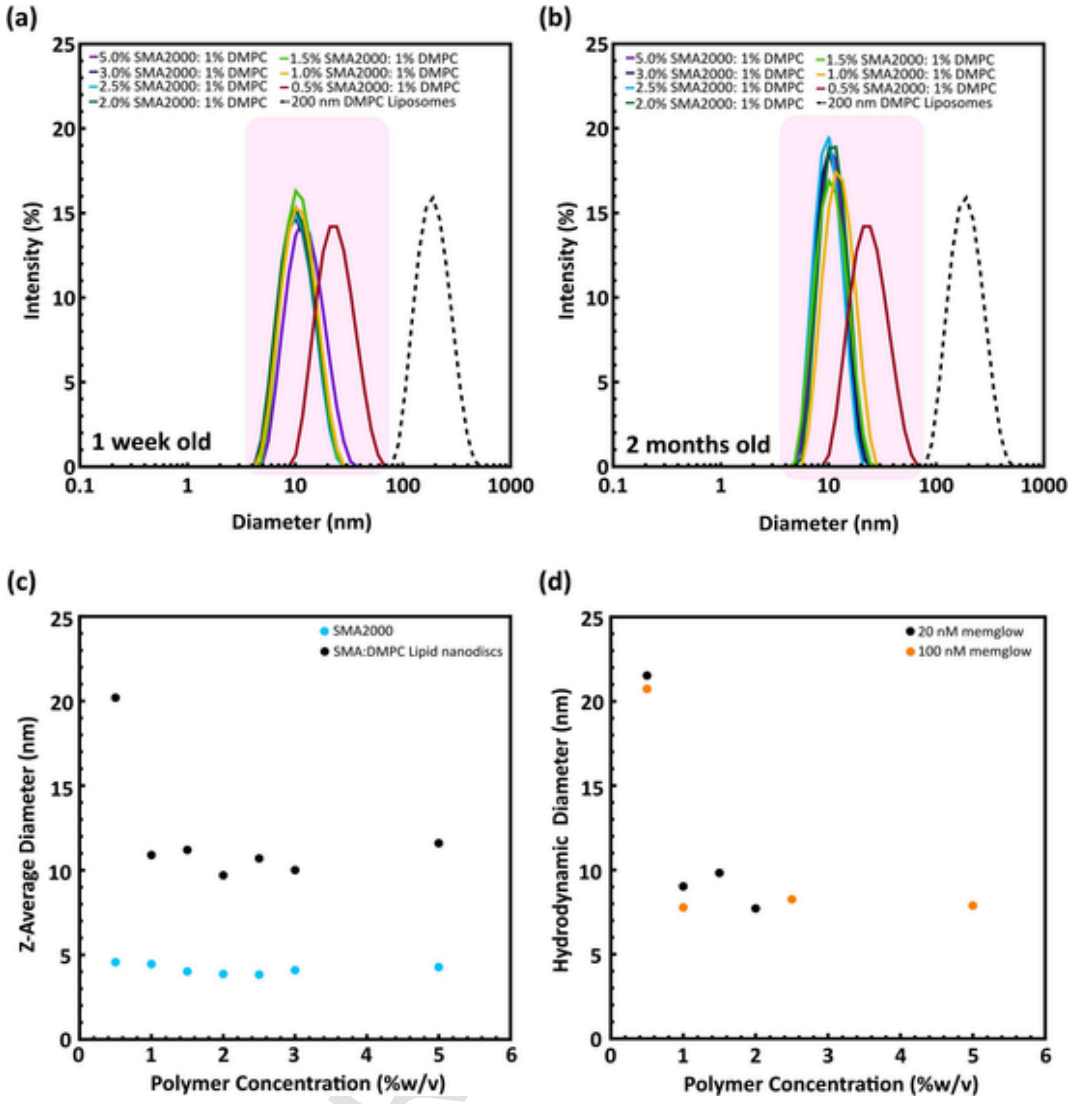

Fig. 5. (a) Dynamic-light scattering of polymer-lipid nanoparticles (1 week after preparation), (b) dynamic-light scattering of polymer-lipid nanoparticles (2 months after preparation), (c) *Z*-average diameter from DLS of polymer (blue) and polymer-lipid nanoparticles (black) with different concentrations of polymer and (d) hydrodynamic diameter measurements from FIDA of polymer-lipid nanoparticles with different concentrations of polymer. Polymer-lipid nanoparticles stained with 20 nM of MemGlow 488 (black) and 100 nM MemGlow 488 (orange). (For interpretation of the references to colour in this figure legend, the reader is referred to the web version of this article.)

(5%) of SMA2000 was used, two populations of polymer–lipid nanoparticles with masses of approximately 50 kDa and 75 kDa were present, with the 50 kDa population being consistent with the additional peak (peak 2 in the SEC highlighted in green). Particles prepared using a low polymer concentration (0.5%) of SMA2000, on the other hand, produced larger particles with masses of approximately 200 kDa and 300 kDa. Overall, SMA2000 based polymer-lipid nanoparticles display multimodal size distributions at very high and at very low polymer-lipid ratios. Polymer-lipid particles produced using 0.5% polymer had a larger mass compared to those prepared using ≥1% SMA2000. This aligns with DLS and FIDA data where 0.5% SMA2000:1% DMPC polymer-lipid nanoparticles were also larger.

SAXS data were similar across the concentration series (Fig. 7(a)), except for the lowest concentrations, consistent with the results from DLS, FIDA and mass photometry. The minimum at $q \sim 0.7$ nm^{-1} shifted to lower values for the samples with polymer-to-lipid ratios below 1.5%, indicating larger particle sizes (Fig. 7(a)), and the scattering from the 0.5% SMA2000 sample displayed a substantially higher slope at low-q, also indicating the presence of larger particles. The data were transformed to yield the pair distance distribution functions (Fig. 7(b)). A characteristic negative contribution was observed around 3 nm, which is a hallmark of a lipid bilayer, with 3 nm being a typical distance between lipid head groups with high electron density and lipid tail groups with low electron density. The samples with low polymer-lipid ratios displayed a tail towards large distances, confirming the presence of larger particles in the sample. Guinier plots (Fig. 7(c)) showed that the slopes and thereby the radii of gyration (R_g) are similar for polymer-lipid ratios above 1.5 (Table 1). Samples with SMA2000:DMPC ratios of 1.0 and 1.5, on the other hand, displayed a visibly steeper slope and higher R_g (Fig. 7(b) and Table 1). Moreover, the Guinier region was not linear for the 0.5 sample, a population of substantially larger particles. Thus, both SAXS data and mass photometry (Fig. 6) indicate the presence of two separate species in the 0.5% SMA2000 sample.

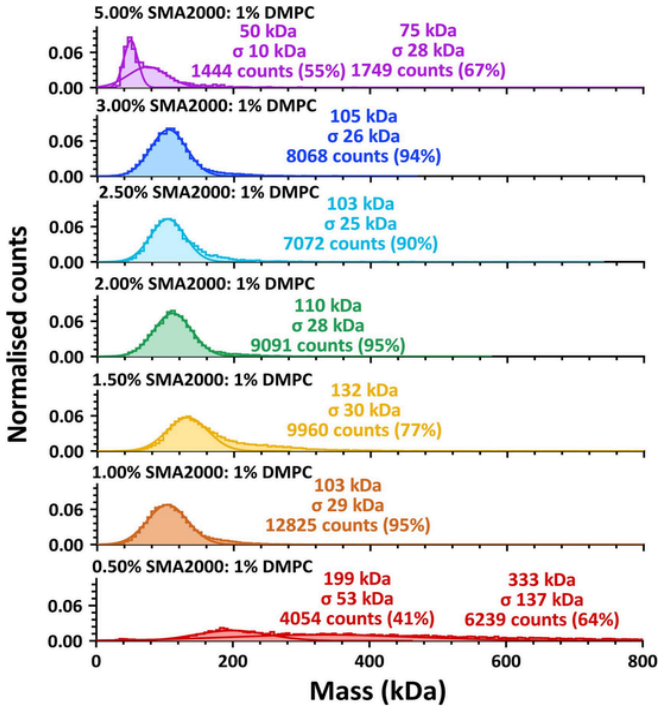

Fig. 6. Mass photometry of SEC purified lipid nanoparticles solubilized with 5%; 3%; 2.5%; 2%; 1.5%; 1.0% and 0.5% SMA2000. NativeMark™ was used for mass calibration. The figure shows the histograms of the purified polymer-lipid nanoparticles with normalized counts plotted against mass. Each histogram peak is fitted with a normal distribution, and labelled with the mean, standard deviation, distribution count and percentage of total sample count.

3.6. Molecular model of SMA2000 nanodiscs with physical constraints

Having established the average size and the multi-modal size distribution of the SMA-lipid nanoparticles, SAXS was used with a new molecular SMALP model to investigate whether SMA nanodiscs [31,48] were formed under all conditions and to probe the particles' stoichiometry. The nanodisc model fitted the data at all investigated polymer-to-lipid ratios (Fig. 7(e) and Table 2).

SMALPs are often prepared with a polymer-to-lipid weight ratio between 2 and 3 (*w*/w) [49,50]. Our results validate this strategy, as in this range, nanodiscs with a consistent size were formed. Each nanodisc contained on average approximately 130 lipids per disc surrounded by 11 polymers (Table 2). This is comparable to a previous SANS study by Jamshad et al. where they estimated that each SMALP contained 140 lipids [18]. Their model, however, does not provide a perfect fit to the data since it decays faster at low and intermediate q values compared to data, meaning that the model returns larger particles than data suggests, possibly compensating for aggregation that is not accounted for in the model. This may explain why this previous work concluded that there were more lipids per nanodisc than we do in this study, which highlights the importance of using SEC-SAXS (or SEC-SANS) for structural studies of dynamic self-assembled particles, or accounting for aggregates in the model [51]. The nanodiscs were found to be polydisperse, and the polymers are also known to be highly polydisperse ($Đ = 2.5$). Therefore, these are average numbers, and no assumptions were made about polymer lengths. Importantly, the nanodisc size and stoichiometry did not change with increasing amounts of SMA2000, if there were sufficient SMA2000 (Fig. 7(g) and Table 2). With insufficient SMA2000, on the other hand, at polymer-lipid ratios below 2.0, the average number of lipids per disc increased with increasing lipid-to-polymer ratio, reaching more than 200 lipids per disc at a polymer–lipid ratio of 0.5. The masses of the polymer-lipid nanoparticles were calculated using the molecular masses of DMPC and SMA2000 (see Supporting Information, Section S6.1), and the masses from SAXS were consistent with the mass photometry data for polymer-to-lipid ratios between 1.5 and 3.0 (Table 1).

3.7. Lipid bilayer height

Using the nanodisc model, it was also possible to address important aspects of SMA nanodisc formation. First, the bilayer structure was investigated. In a previous study by Maier et al. [48], it was suggested that the bilayer height of SMALPs varied with polymer to lipid ratio. However, our modelling suggested a constant bilayer height (Table 2), as supported by visual inspection of the pair distance distributions, where the minima were all within a few tenths of a nanometer (Fig. 7 (b)). A validity check of our model was be done by comparing the lipid tail group height to the lipid head group height, as refined from the model (Table 2) and illustrated in Fig. 7(f). The height of the lipid tail group was 2.43 times the lipid head height, and thereby consistent with the ratio of their respective molecular volumes (see Supporting Information, Table S6.1.3), which was 2.46. The observations in Maier et al. [48], may be affected by sample preparation, as their SAXS data at low polymer-lipid ratios, did not display a well-resolved Guinier region and had a large d_{max} in the pair distance distribution (up to 50 nm). Those are signs of a larger population in the sample, which could be liposomes [31], or large nanodiscs coexisting with smaller nanodiscs. Increased polydispersity shifts the minimum in the $p(r)$ to higher distances, which can explain their observations without assuming a change in bilayer height. Finally, in their nanodisc model, the same electron density or scattering length density (SLD) was used for lipid head group and polymer belt, namely $800{\cdot}10^{-6}$ Å^{-2}. Our best estimate is that the SLD for SMA2000 is around $11{\cdot}10^{-6}$ Å^{-2} and the SLD for the lipid headgroup is approximately $13{\cdot}10^{-6}$ Å^{-2} (converted from ED to SLD for ease of comparison, SI section 6.1). These differences points to the importance of reporting how electron densities or SLD values are calculated. For these reasons, we believe that the bilayer thickness in the SMALPs remains constant, despite changes in polymer-lipid ratio. Jamshad et al. [18] investigated SMALPs comprising SMA2000 and DMPC using SANS, and found a lipid tail group height of 2.6 ± 0.2 nm, consistent with our value of 2.4 nm, but estimated the total lipid head group height to be 2.0 ± 0.4 nm, twice the value reported here and thus not consistent with the volume ratios of tail and head groups in DMPC, as described above. Such deviation was not possible in our model due to the applied molecular constraints. Our results are consistent with the Gibbs-Luzzati bilayer thickness [52] modified by a roughness term to account for a Gaussian lipid-water interface, which is appropriate for models without significant hydration of the lipid headgroups. A larger effective headgroup is possible after substantial hydration, which should be accounted for in the electron densities (or scattering length densities in SANS), and in that case the relevant reference value is the steric bilayer thickness, which is consistent with the results reported by Jamshad et al. [18]

3.8. Localization of SMA2000 in the discs

The molecular model also provides insight into the distribution of SMA in the nanodiscs, in particular whether they are mixed into the lipid bilayer or confined to the rim as illustrated in Fig. 7(f). Bjornstad et al. [31] reports that their nanodisc data cannot be modelled accurately without a fraction of SMA mixed into the lipid headgroups. Contrary to that, the data was accurately modelled with SMA only present in the belt. From the data, it cannot be excluded that there could be some SMA inserted in the lipid bilayer, with styrene among the lipid tails and maleic acid in the lipid head groups as suggested by Bjornstad et al., as this would not drastically change the electron density distribu-

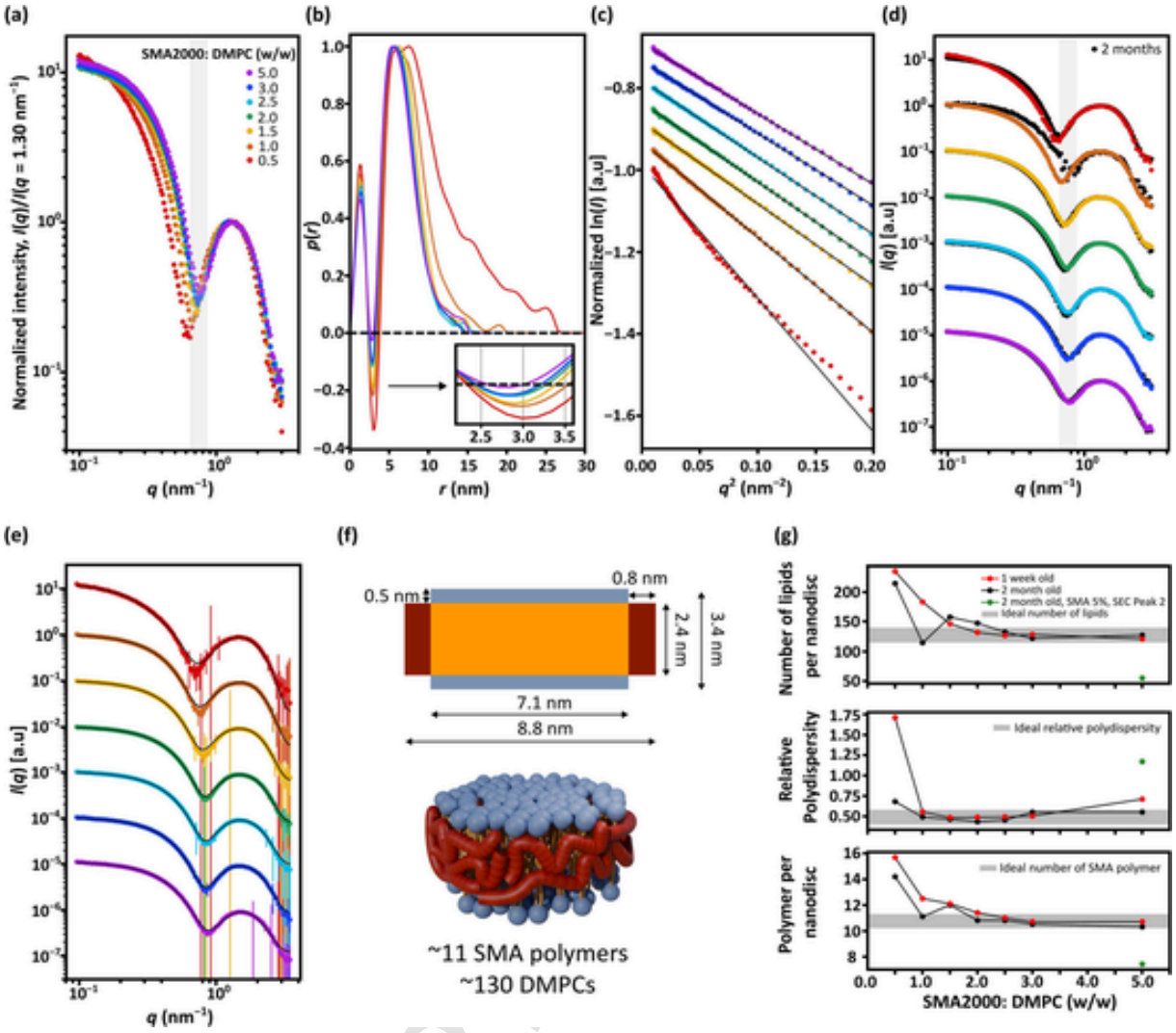

Fig. 7. (a) SAXS data of SMA2000-DMPC nanoparticles (1 week old samples). They grey bar shows the position of the local minimum for samples with a 1.5 SMA2000:DMPC (*w*/w) ratio or higher. (b) Normalized pair distance distribution functions, *p(r)*, with insert showing the minimum around 3 nm, indicative of the bilayer height. (c) Guinier plots and fits (black). The data were shifted along the y-axis to avoid overlap. (d) 2-month-old data in black compared to the 1-week-old. (e) 1-week old samples fitted with polydisperse nanodiscs model (f) illustration and dimension of the average SMA2000:DMPC nanodisc. Dimensions are average of the refined values for SMALPs with polymer-to-lipid ratios of 2.0, 2.5 and 3.0 all rounded to 1 decimal place (Table 2). The polymer chains are polydisperse so while there may be more or fewer chains in a given nanodisc, this is the number of chains with the average degree of polymerization. (g) Change of key parameters such as function of polymer to lipid ratio in the samples. If sufficient SMA2000 is present (ratios of 2.0 or 2.5 and above, a stable "plateau" is reached (grey). At high SMA2000 concentration, an additional peak (Peak 2) appeared in the SEC (Fig. 4). This peak can be fitted with a small nanodisc (Fig. S6.3.3), with parameters represented by the green dots.

tion (see Supporting Information, Table S6.1.3). However, it can be positively stated that a model with SMA only in the rim, as illustrated in Fig. 7(f), is consistent with our data. Moreover, insertion of amphiphiles in lipid bilayers typically induce curvature, via a wedge-like mechanism [53]. This explains why SMA insertion reduce vesicle size, spontaneously forming liposomes with diameters as small as 50 nm [31]. However, due to the flat geometry of the lipid bilayer in nanodiscs, as opposed to the curved nature of small liposomes, it is energetically more favourable for the SMA to form the polymer belt of the nanodiscs. This is further supported by molecular dynamics simulations of SMALP self-assembly, where SMA was also localized in the rim in mature nanodiscs [54]. Taken together, we assessed that a nanodisc with SMA2000 localized only at the rim was the most accurate SMALP model.

3.9. Polymer belt width

The SAXS data and modelling also gave important insights into the polymer belt formation and highlight a potential pitfall in the modelling of nanodiscs with SAXS. The SMALP SAXS data could be fitted with two different polymer belt sizes: one model has a 0.8 nm polymer belt corresponding to a single layer of SMA (Fig. 7 and Table 2), the other model had a 1.5 nm wide belt (Fig. S6.3.2 and Table S6.3.2). The thickness of the polymer belt is also comparable with a similar SMA polymer belt measured using small-angle neutron scattering (SANS) [18]. A similarly wide belt was reported by Bjornestad et al. [31] for DMPC at 18 °C at 0.5% SMA (3,1) and 1% DMPC concentration (polymer lipid ratio of 0.5). However, due to the chemical structure, molecular dimensions and amphipathic nature of SMA2000, the 0.8 nm belt appears most realistic, as it is consistent with a single layer of SMA, having the styrene groups closely packed among the lipid tails, and the hydrophilic

Table 1
SMALPs size estimation from DLS, FIDA, mass photometry and SAXS, uncertainties are standard deviations.

SMA2000:DMPC ratio	0.5	1.0	1.5	2.0	2.5	3.0	5.0
DLS							
Hydrodynamic diameter (nm) (PDI)	20.2 (0.18)	10.9 (0.12)	11.2 (0.08)	9.7 (0.11)	10.7 (0.20)	10.0 (0.16)	11.6 (0.14)
FIDA							
Hydrodynamic diameter (nm)	21.53 ± 0.18 /	9.03 ±	9.83 ±	7.72 ±	−/	−/−	−/
20 mM/100 mM MemGlow 488	20.73 ± 0.06	0.06/	0.03/	0.01/	8.26 ±		7.89 ±
		7.78 ± 0.06	-	-	0.04		0.03
SAXS primary data analysis							
d_{max} (nm)	26.4 ± 0.3	19.8 ± 0.3	15.3 ± 0.3	14.6 ± 0.3	15.8 ± 0.7	14.7 ± 0.5	15.0 ± 0.2
R_g (nm)	8.99 ± 0.02	5.50 ± 0.02	4.92 ± 0.01	4.69 ± 0.01	4.69 ± 0.01	4.67 ± 0.01	4.75 ± 0.01
SAXS nanodisc model							
Disc diameter (nm)	11.4 ± 1.3	10.1 ± 1.3	9.2 ± 1.1	8.8 ± 1.1	8.7 ± 1.1	8.7 ± 1.1	8.6 ± 1.0
Bilayer height (nm)	3.40 ± 0.04	3.38 ± 0.04	3.42 ± 0.04	3.41 ± 0.04	3.38 ± 0.04	3.38 ± 0.04	3.40 ± 0.04
Mass (kDa)	209 ± 9	164 ± 4	138 ± 3	126 ± 3	122 ± 3	121 ± 3	117 ± 3
Mass photometry							
Mass	199 ± 53	103 ± 29	132 ± 30	110 ± 28	103 ± 25	105 ± 26	50 ± 10
(kDa)	333 ± 137						75 ± 28

Table 2
Refined and derived parameters for the SMA nanodisc models. N_{lip}: number of lipids per nanodisc; $\sigma_{pd,rel}$: relative polydispersity in the number of lipids; σ_R: roughness; T: thickness of polymer belt; Adjust $V_{tail/head/SMA}$: correction factors for lipid tail volum/lipid head volume/SMA volumes; $N_{polymers}$: number of polymers per nanodisc; H_{core}: height of lipid core; H_{head}: height of the two lipid head groups.

Polymer/lipid ratio (w/w)	0.5	1.0	1.5	2.0	2.5	3.0	5.0
N_{lip}	234 ± 13	183 ± 5	146 ± 4	132 ± 4	127 ± 4	128 ± 4	121 ± 4
$\sigma_{pd,rel}$	1.7 ± 0.1	0.55 ± 0.01	0.48 ± 0.07	0.49 ± 0.05	0.49 ± 0.06	0.50 ± 0.07	0.71 ± 0.01
σ_R (nm)	0.97 ± 0.02	0.94 ± 0.01	0.90 ± 0.02	0.96 ± 0.01	0.95 ± 0.02	0.95 ± 0.02	1.00 ± 0.02
T (nm)	0.9 ± 0.1	0.8 ± 0.1	0.8 ± 0.1	0.8 ± 0.1	0.8 ± 0.1	0.8 ± 0.1	0.8 ± 0.1
Adjust V_{tail}	0.94 ± 0.01	0.95 ± 0.01	0.95 ± 0.01	0.95 ± 0.01	0.95 ± 0.01	0.95 ± 0.01	0.94 ± 0.01
Adjust V_{head}	0.97 ± 0.01	0.98 ± 0.01	0.97 ± 0.01	0.98 ± 0.01	0.96 ± 0.01	0.98 ± 0.01	0.97 ± 0.01
Adjust V_{SMA}	1.02 ± 0.01	0.97 ± 0.02	0.95 ± 0.02	0.96 ± 0.02	0.95 ± 0.02	0.96 ± 0.02	0.98 ± 0.01
Adjust A_{lip}	1.01 ± 0.01	1.03 ± 0.01	1.02 ± 0.01	1.04 ± 0.01	1.03 ± 0.01	1.03 ± 0.01	1.02 ± 0.01
Derived/calculated							
$N_{polymers}$	15.7 ± 0.5	12.5 ± 0.3	12.1 ± 0.3	11.4 ± 0.3	11.0 ± 0.3	10.7 ± 0.3	10.7 ± 0.2
Diameter (nm)	11.4 ± 1.3	10.1 ± 1.3	9.2 ± 1.1	8.8 ± 1.1	8.7 ± 1.1	8.7 ± 1.1	8.6 ± 1.0
H_{core} (nm)	2.40 ± 0.03	2.38 ± 0.03	2.42 ± 0.03	2.43 ± 0.03	2.39 ± 0.03	2.38 ± 0.03	2.40 ± 0.03
H_{head} (nm)	1.00 ± 0.05	1.00 ± 0.05	1.00 ± 0.05	0.98 ± 0.05	0.99 ± 0.05	1.00 ± 0.05	1.00 ± 0.05
Goodness of fit							
χ^2	3.8	6.6	3.5	4.2	4.0	3.2	2.8

maleic acid groups facing the surrounding water phase. This narrow polymer belt model is also consistent with in silico studies of self-assembled SMA nanodiscs [54].

3.10. Tiny SMA nanodiscs at high polymer-to-lipid-ratios

At the highest polymer-to-lipid ratio (5.0), the SMALPs were distributed into two distinct species (Fig. 4), one nanodisc with the "ideal" stoichiometry (SEC peak 1, highlighted in pink, Fig. 4), and a smaller species (SEC peak 2, highlighted in green, Fig. 4). The second peak was also seen as a shoulder at lower polymer-to-lipid ratios. The particle size from this second peak was analysed with DLS and displayed a hydrodynamic diameter of ~8 nm (PDI = 0.13), smaller than ~10 nm (PDI = 0.1) for the ideal nanodiscs (Fig. S5.4.1). Mass photometry was also indicative of the presence of smaller species in the sample with mass 50 ± 10 kDa. SAXS data from the sample could be fitted with a small nanodisc (Fig. S6.3.3), with only 55 lipids and 7 polymer chains compared to 130 lipids and 11 polymers in the nanodiscs with most stable stoichiometry. The mass of a polymer-lipid nanoparticle with 55 lipids and 7 polymers was calculated to be ~60 kDa. Thus, both SAXS and mass photometry suggested that when there is excess polymer in the system, some smaller nanodiscs are produced in addition to the main population of 'ideal' nanodiscs. The relative proportion of SMA2000 to DMPC was high in these tiny SMA nanodiscs (as they have a larger circumference-to-volume ratio), thereby the tiny nanodiscs effectively functioned as a polymer reservoir for excess SMA2000.

3.11. At low polymer-to-lipid ratios two nanodisc populations with distinct sizes co-exist

As demonstrated by mass photometry (Fig. 6) and analysis of the SAXS Guinier region (Fig. 7(c)), there appears to be two distinctive particle sizes present in the sample with the lowest polymer-to-lipid ratio of 0.5. At this ratio, it has previously been shown that SMALPs and small liposomes (down to 50 nm diameter) with bound SMA co-exist [31]. However, data was obtained using SEC-SAXS, where even small liposomes are separated from the nanodiscs. So, instead we hypothesized that the sample contained two nanodiscs populations, significantly different in size. The pair distance distribution for the sample with a polymer-to-lipid ratio of 0.5 displayed two maxima, the first one aligned with the maxima of the other samples, but the second one was shifted to larger distances and indicated the presence of a population of larger nanodiscs. We could fit the data accurately with a fraction of larger nanodiscs added to the model (Fig. S6.3.4), with 4.7 times more lipids, corresponding to a two-fold increase in nanodisc diameter from 11.4 nm to 22.8 nm (Table S6.3.3). All other parameters, except scaling in the number of lipids, were kept at the same value for the two nanodisc populations to avoid overfitting the data. A fraction of 0.43 of the

scattering was predicted to come from the larger nanodisc population. Using this bimodal nanodisc model, the relative polydispersity was decreased from 1.7 to a more reasonable value of 0.3, and the χ^2 value decreased from 3.8 to 1.1. The bimodal nanodisc model also improved the fit to the samples with a polymer-to-lipid ratio of 1.0, although in this case, the pair distribution function only showed a shoulder rather than a distinct secondary peak. In accordance with this observation, the scattering-weighted fraction of larger nanodiscs were only 0.2 in this case, and the larger nanodiscs had only 3.2 times more lipids.

3.12. Stability of SMALPs

One set of SMALPs was prepared two months prior to the SAXS measurements and stored at 5 °C. Another set of samples were freshly prepared, 1 week prior to the measurements, also stored at 5 °C. The 2-month old samples were very similar to the 1-week samples for polymer-to-lipid ratios between 1.5 and 5.0 (Fig. 7(d)), i.e. with sufficient SMA2000. This long-term stability was consistent with the SEC (Fig. 4) and DLS (Fig. 5(a-b)) data. Both sets of SEC data exhibited similar trends, especially at the higher concentrations of SMA2000. However, DLS did show small changes over time for the 0.5% SMA2000 sample, which reduced in size from ~20 nm (PDI = 0.18) to ~16 nm (PDI = 0.13) after 2 months. This was also observed in the SAXS data; for the lowest ratios of 0.5 and 1.0, the minimum in the scattering curves shifted towards smaller sizes, i.e. towards the size that is seen as the samples prepared with sufficient SMA content. This demonstrates that the SMA2000-DMPC nanodiscs are very stable over time if they are prepared with sufficient SMA2000 such as when ratios of SMA2000: DMPC are greater than 1.5.

4. Conclusions

A suite of characterization techniques was employed to systematically investigate the structural consequences (size, shape and stability) of polymer-lipid nanoparticles formed using varying concentrations of SMA2000 with a constant concentration of DMPC. Both DLS and FIDA measurements show that SMALPs formed at SMA2000 concentrations above 1.5% exhibit hydrodynamic diameters of approximately 10 nm, consistent with the characteristic dimensions of SMALPs reported in the literature. It was found that the 'ideal' polymer to lipid ratio for forming SMALP nanodiscs is between 2.0 and 3.0, and in this range, the SMALP nanodiscs size and polymer to lipid ratio is close to constant. Based on our refined SAXS model it was found that SMA2000 and DMPC form nanodiscs with approximately 130 lipids and 11 polymer chains on average, despite the high molecular weight polydispersity of the polymers. That corresponds to a mass of ~123 ± 5 kDa which is comparable with the mass measured using mass photometry of 106 ± 45 kDa. The SMALP nanodiscs were structurally very stable over time (at least 2 months), if prepared with sufficient SMA2000. At lower polymer:lipid ratios, i.e. below 1.5:1, we report for the first time that SMALP nanodiscs coexist with a larger nanodisc population with a relatively low proportion of SMA2000. At higher polymer:lipid ratios, smaller SMALPs with a relatively high SMA content are formed along with the 'ideal' SMALP nanodiscs. These small nanodiscs are stabilised by some of the excess SMA2000, while some remaining SMA2000 chains form polymer assemblies without lipids. Overall, this suggests SMALPs have a preferred size range, and major deviations in polymer to lipid ratios used in the preparation leads to bimodal size distributions rather than a continuous increase or decrease in the size in the predominant nanodisc population.

CRediT authorship contribution statement

Bridget Tang: Writing – review & editing, Writing – original draft, Visualization, Validation, Methodology, Investigation. **Philip Kitchen:** Writing – review & editing, Investigation, Formal analysis. **Luke M. Broadbent:** Writing – review & editing, Investigation. **Steven D. Quinn:** Writing – review & editing, Investigation, Formal analysis. **Nawal Hassan:** Writing – review & editing, Investigation. **Siriporn Chaimueangchuen:** Writing – review & editing, Investigation. **Barbara Gerbelli:** Writing – review & editing, Investigation. **Katsuaki Inoue:** Investigation. **Nathan Cowieson:** Investigation. **Fátima Herranz-Trillo:** Investigation. **Alice J. Rothnie:** Writing – review & editing, Supervision, Funding acquisition, Formal analysis, Conceptualization. **Roslyn M. Bill:** Writing – review & editing, Supervision, Funding acquisition. **Paul D. Topham:** Writing – review & editing, Supervision, Funding acquisition, Formal analysis, Conceptualization. **Alan D. Goddard:** Writing – review & editing, Supervision, Funding acquisition, Formal analysis, Conceptualization. **Jacob J.K. Kirkensgaard:** Writing – review & editing, Supervision, Funding acquisition, Conceptualization. **Matthew J. Derry:** Writing – review & editing, Supervision, Investigation, Funding acquisition, Formal analysis, Conceptualization. **Andreas Haahr Larsen:** Writing – review & editing, Writing – original draft, Visualization, Methodology, Investigation, Formal analysis.

Declaration of competing interest

The authors declare that they have no known competing financial interests or personal relationships that could have appeared to influence the work reported in this paper.

Acknowledgements

M.J.D. and A.D.G. wish to thank EPSRC (grant number EP/Y001443/1). This project also received funding from the European Union's Horizon Europe research and innovation program under grant agreement No 101124675 and UKRI (UK Research and Innovation) grant agreement No 10112970 (BIOMEM.eu). J.J.K.K. acknowledges support from the Danish Agency for Higher Education and Science (ESS Lighthouse: Colloids and Interfaces in Food and Pharma; Grant No. 726510). SDQ thanks EPSRC (EP/V034030/1) for support. R.M.B. is supported by UKRI Frontier Research Grant EP/Y023684/1 (following assessment as an ERC Advanced grant, FORTIFY, ERC-2022-ADG-101096882 under the UK Government Guarantee scheme) and acknowledges a Biotechnology and Biological Sciences Research Council Pioneer Award (BB/Y512874/1) and a Visiting Fellowship at Corpus Christi College, University of Oxford. Small-angle X-ray scattering (SAXS) experiments were conducted with the support of Diamond Light Source, instrument B21 (proposal SM39511-1). A.H.L. and J.J.K.K. gratefully acknowledge financial support from DanScatt. We thank Raider Lund, Victoria Bjørnestad, Karen Edler and George Neville for input and discussion on polymer ED determination and SAXS modelling aspects. We thank Minmin Xue and Siewert Jan Marrink for providing MD coordinates for SMA [54]. We authors thank Jo Walter (Fidabio) for facilitating the long-term loan of a Fida1 instrument and Thomas Bedwell (Fidabio) for technical support. The Aston Institute for Membrane Excellence (AIME) is funded by UKRI's Research England as part of their Expanding Excellence in England (E3) fund.

Data availability

All 1D reduced SAXS data are openly available at github.com/andreashlarsen/Tang2025. Any other data can be provided upon request.

Appendix A. Supplementary data

Supplementary data to this article can be found online at https://doi.org/10.1016/j.jcis.2026.141054.

References

[1] S. Tan, H.T. Tan, M.C. Chung, Proteomics 8 (19) (2008) 3924–3932, https://doi.org/10.1002/pmic.200800597.
[2] I.A. Smirnova, P. Ädelroth, P. Brzezinski, Sci. Rep. 8 (1) (2018) 14950, https://doi.org/10.1038/s41598-018-33208-1.
[3] A.M. Seddon, P. Curnow, P.J. Booth, Biochim. Biophys. Acta (BBA)-Biomembr. 1666 (1–2) (2004) 105–117, https://doi.org/10.1016/j.bbamem.2004.04.011.
[4] T.J. Knowles, R. Finka, C. Smith, Y.-P. Lin, T. Dafforn, M. Overduin, J. Am. Chem. Soc. 131 (22) (2009) 7484–7485, https://doi.org/10.1021/ja810046q.
[5] G.C. Kuyler, E. Barnard, R.D. Cunningham, S. Sibariboyi, L. White, I. Wessels, M.-P. Smith, B. Motloung, B. Klumperman, The Journal of Physical Chemistry Letters 16 (23) (2025) 5784–5799, https://doi.org/10.1021/acs.jpclett.5c00680.
[6] M.-P. Smith, L.E. Ball, B. Klumperman, Macromolecules 58 (15) (2025) 8409–8418, https://doi.org/10.1021/acs.macromol.5c01372.
[7] G.M. Neville, K.A. Morrison, E.R. Shilliday, J. Doutch, R. Dalgliesh, G.J. Price, K.J. Edler, Soft Matter 19 (44) (2023) 8507–8518, https://doi.org/10.1039/D3SM01180A.
[8] R.D. Cunningham, A.H. Kopf, B.O. Elenbaas, B.B. Staal, R. Pfukwa, J.A. Killian, B. Klumperman, Biomacromolecules 21 (8) (2020) 3287–3300, https://doi.org/10.1021/acs.biomac.0c00736.
[9] S.C. Hall, C. Tognoloni, G.J. Price, B. Klumperman, K.J. Edler, T.R. Dafforn, T. Arnold, Biomacromolecules 19 (3) (2017) 761–772, https://doi.org/10.1021/acs.biomac.7b01539.
[10] Kopf, A. H.; Koorengevel, M. C.; van Walree, C. A.; Dafforn, T. R.; Killian, J. A. Chem. Phys. Lipids 2019, 218, 85–90. DOI: https://doi.org/10.1016/j.chemphyslip.2018.11.011 DOI: 10.1016/j.chemphyslip.2018.11.011.
[11] T. Khaojanta, P. Punyamoonwongsa, R. Molloy, J. Appl. Polym. Sci. 141 (28) (2024) e55641, https://doi.org/10.1002/app.55641.
[12] E. Tsuchida, T. Tomono, Die Makromolekulare Chemie: Macromol. Chem. Phys. 141 (1) (1971) 265–298, https://doi.org/10.1002/macp.1971.021410122.
[13] S. Bag, S. Ghosh, S. Paul, M.E.H. Khan, P. De, Macromol. Rapid Commun. 42 (23) (2021) 2100501, https://doi.org/10.1002/marc.202100501.
[14] A.A. Gulamhussein, R. Uddin, B.J. Tighe, D.R. Poyner, A.J. Rothnie, Biochim. Biophys. Acta (BBA)-Biomembr. 1862 (7) (2020) 183281, https://doi.org/10.1016/j.bbamem.2020.183281.
[15] N.L. Pollock, S.C. Lee, J.H. Patel, A.A. Gulamhussein, A.J. Rothnie, Biochim. Biophys. Acta (BBA)-Biomembr. 1860 (4) (2018) 809–817, https://doi.org/10.1016/j.bbamem.2017.08.012.
[16] S. Gulati, M. Jamshad, T.J. Knowles, K.A. Morrison, R. Downing, N. Cant, R. Collins, J.B. Koenderink, R.C. Ford, M. Overduin, Biochem. J. 461 (2) (2014) 269–278, https://doi.org/10.1042/BJ20131477.
[17] S.J. Hesketh, D.P. Klebl, A.J. Higgins, M. Thomsen, I.B. Pickles, F. Sobott, A. Sivaprasadarao, V.L. Postis, S.P. Muench, Biochim. Biophys. Acta (BBA)-Biomembr. 1862 (5) (2020) 183192, https://doi.org/10.1016/j.bbamem.2020.183192.
[18] M. Jamshad, V. Grimard, I. Idini, T.J. Knowles, M.R. Dowle, N. Schofield, P. Sridhar, Y. Lin, R. Finka, M. Wheatley, Nano Res. 8 (3) (2015) 774–789, https://doi.org/10.1007/s12274-014-0560-6.
[19] H. Sawczyc, S. Heit, A. Watts, Eur. Biophys. J. 52 (1) (2023) 39–51, https://doi.org/10.1007/s00249-023-01632-5.
[20] J.M. Dörr, M.C. Koorengevel, M. Schäfer, A.V. Prokofyev, S. Scheidelaar, E.A. Van Der Cruijsen, T.R. Dafforn, M. Baldus, J.A. Killian, Proc. Natl. Acad. Sci. USA 111 (52) (2014) 18607–18612, https://doi.org/10.1073/pnas.1416205112.
[21] O.P. Hawkins, T.J. Potter, L.M. Broadbent, P. Kitchen, A.D. Goddard, A.J. Rothnie, Biosci. Rep. 46 (2) (2026) BSR20250256, https://doi.org/10.1042/BSR20250256.
[22] L. Unger, A. Ronco-Campaña, P. Kitchen, R.M. Bill, A.J. Rothnie, Biochem. Soc. Trans. 49 (3) (2021) 1349–1359, https://doi.org/10.1042/BST20201067.
[23] A.A. Smith, H.E. Autzen, B. Faust, J.L. Mann, B.W. Muir, S. Howard, A. Postma, A.J. Spakowitz, Y. Cheng, E.A. Appel, Chem 6 (10) (2020) 2782–2795, https://doi.org/10.1016/j.chempr.2020.08.004.
[24] J. Lenz, A.H. Larsen, S. Keller, A. Luchini, Langmuir 39 (10) (2023) 3569–3579, https://doi.org/10.1021/acs.langmuir.2c03019.
[25] K. Yasuhara, J. Arakida, T. Ravula, S.K. Ramadugu, B. Sahoo, J.-i. Kikuchi, A. Ramamoorthy, J. Am. Chem. Soc. 139 (51) (2017) 18657–18663, https://doi.org/10.1021/jacs.7b10591.
[26] S. Perrier, Macromolecules 50 (19) (2017) 7433–7447, https://doi.org/10.1021/acs.macromol.7b00767.
[27] G. Moad, E. Rizzardo, S.H. Thang, Acc. Chem. Res. 41 (9) (2008) 1133–1142, https://doi.org/10.1021/ar800075n.
[28] E. Kamilar, J. Bariwal, W. Zheng, H. Ma, H. Liang, Biomacromolecules 24 (4) (2023) 1819–1838, https://doi.org/10.1021/acs.biomac.3c00034.
[29] R.C. Arenas, J. Klingler, C. Vargas, S. Keller, Nanoscale 8 (32) (2016) 15016–15026, https://doi.org/10.1039/C6NR02089E.
[30] A.F. Craig, E.E. Clark, I.D. Sahu, R. Zhang, N.D. Frantz, M.S. Al-Abdul-Wahid, C. Dabney-Smith, D. Konkolewicz, G.A. Lorigan, Biochim. Biophys. Acta (BBA)-Biomembr. 1858 (11) (2016) 2931–2939, https://doi.org/10.1016/j.bbamem.2016.08.004.
[31] V.A. Bjørnestad, M. Orwick-Rydmark, R. Lund, Langmuir 37 (20) (2021) 6178–6188, https://doi.org/10.1021/acs.langmuir.1c00304.
[32] P.A. Dalgarno, J. Juan-Colás, G.J. Hedley, L. Piñeiro, M. Novo, C. Perez-Gonzalez, I.D. Samuel, M.C. Leake, S. Johnson, W. Al-Soufi, Sci. Rep. 9 (1) (2019) 12897, https://doi.org/10.1038/s41598-019-49210-0.
[33] J. Juan-Colas, L. Dresser, K. Morris, H. Lagadou, R.H. Ward, A. Burns, S. Tear, S. Johnson, M.C. Leake, S.D. Quinn, Langmuir 36 (39) (2020) 11499–11507, https://doi.org/10.1021/acs.langmuir.0c01810.
[34] L. Dresser, S.P. Graham, L.M. Miller, C. Schaefer, D. Conteduca, S. Johnson, M.C. Leake, S.D. Quinn, The Journal of Physical Chemistry Letters 13 (23) (2022) 5341–5350, https://doi.org/10.1021/acs.jpclett.2c00704.
[35] N.P. Cowieson, C.J. Edwards-Gayle, K. Inoue, N.S. Khunti, J. Doutch, E. Williams, S. Daniels, G. Preece, N.A. Krumpa, J.P. Sutter, Synchrotron Radiat. 27 (5) (2020) 1438–1446, https://doi.org/10.1107/S1600577520009960.
[36] J. Filik, A.W. Ashton, P.C.Y. Chang, P. Chater, S. Day, M. Drakopoulos, M. Gerring, M. Hart, O. Magdysyuk, S. Michalik, J. Appl. Crystallogr. 50 (3) (2017) 959–966, https://doi.org/10.1107/S1600576717004708.
[37] A.H. Larsen, M.C. Pedersen, J. Appl. Crystallogr. 54 (5) (2021) 1281–1289, https://doi.org/10.1107/S1600576721006877.
[38] J. Trewhella, P. Vachette, A.H. Larsen, IUCrJ 11 (5) (2024) 762–779, https://doi.org/10.1107/S205225252400486X.
[39] J.B. Hopkins, J. Appl. Crystallogr. 57 (1) (2024) 194–208, https://doi.org/10.1107/S1600576723011019.
[40] E. Brookes, P. Vachette, M. Rocco, J. Pérez, J. Appl. Crystallogr. 49 (5) (2016) 1827–1841, https://doi.org/10.1107/S1600576716011201.
[41] S. Hansen, Appl. Crystallogr. 33 (6) (2000) 1415–1421, https://doi.org/10.1107/S0021889800012930.
[42] A.H. Larsen, L. Arleth, S. Hansen, Appl. Crystallogr. 51 (4) (2018) 1151–1161, https://doi.org/10.1107/S1600576718008956.
[43] A.H. Larsen, Appl. Crystallogr. 58 (3) (2025) 934–947, https://doi.org/10.1107/S1600576725002390.
[44] N.G. Brady, S. Qian, B.D. Bruce, Eur. Polym. J. 111 (2019) 178–184, https://doi.org/10.1016/j.eurpolymj.2018.11.034.
[45] S. Scheidelaar, M.C. Koorengevel, J.D. Pardo, J.D. Meeldijk, E. Breukink, J.A. Killian, Biophys. J. 108 (2) (2015) 279–290, https://doi.org/10.1016/j.bpj.2014.11.3464.
[46] L. Broadbent, P. Depping, A. Lodé, A. Vaitsopoulou, D. Hardy, H. Ayub, J. Mitchell-White, I.D. Kerr, A.D. Goddard, R.M. Bill, Detergent-free membrane protein purification using SMA polymer, in: Heterologous Expression of Membrane Proteins: Methods and Protocols, Springer, 2022, pp. 389–404, https://doi.org/10.1007/978-1-0716-2368-8_21.
[47] M.E. Pedersen, J. Østergaard, H. Jensen, Flow-induced dispersion analysis (FIDA) for protein quantification and characterization, in: Clinical Applications of Capillary Electrophoresis: Methods and Protocols, Springer, 2019, pp. 109–123, https://doi.org/10.1007/978-1-4939-9213-3_8.
[48] R. Maier, R. Cuevas Arenas, F. Zhang, A. Garcia-Saez, F. Schreiber, Langmuir 39 (6) (2023) 2450–2459, https://doi.org/10.1021/acs.langmuir.2c03412.
[49] H. Ayub, M. Clare, I. Milic, N.P. Chmel, H. Böning, A. Devitt, T. Krey, R.M. Bill, A.J. Rothnie, Biochim. Biophys. Acta (BBA)-Biomembr. 1862 (11) (2020) 183419, https://doi.org/10.1016/j.bbamem.2020.183419.
[50] K.A. Morrison, A. Akram, A. Mathews, Z.A. Khan, J.H. Patel, C. Zhou, D.J. Hardy, C. Moore-Kelly, R. Patel, V. Odiba, Biochem. J. 473 (23) (2016) 4349–4360, https://doi.org/10.1042/BCJ20160723.
[51] A.H. Larsen, J.S. Pedersen, L. Arleth, Appl. Crystallogr. 53 (4) (2020) 991–1005, https://doi.org/10.1107/S1600576720006500.
[52] J.F. Nagle, S. Tristram-Nagle, Biochim. Biophys. Acta (BBA)-Rev. Biomembr. 1469 (3) (2000) 159–195, https://doi.org/10.1016/s0304-4157(00)00016-2.
[53] H.T. McMahon, J.L. Gallop, Nature 438 (7068) (2005) 590–596, https://doi.org/10.1038/nature04396.
[54] M. Xue, L. Cheng, I. Faustino, W. Guo, S.J. Marrink, Biophys. J. 115 (3) (2018) 494–502, https://doi.org/10.1016/j.bpj.2018.06.018.